Journal of Power Sources 184 (2008) 172–179

Contents lists available at ScienceDirect

Journal of Power Sources

journal homepage: www.elsevier.com/locate/jpowsour

$MnCo_{1.9}Fe_{0.1}O_4$ spinel protection layer on commercial ferritic steels for interconnect applications in solid oxide fuel cells

X. Montero[a,b,*], F. Tietz[b], D. Sebold[b], H.P. Buchkremer[b], A. Ringuede[c], M. Cassir[c], A. Laresgoiti[a], I. Villarreal[a]

[a] Ikerlan-Energia, Parque Tecnologico de Alava, Juan de La Cierva 1, 01501 Miñano, Spain
[b] Jülich Forschungszentrum, Institute for Materials and Processes in Energy Systems, 52428 Jülich, Germany
[c] LECA UMR7575, ENSCP, 11 rue Pierre et Marie Curie, 75231 Paris cedex 05, France

ARTICLE INFO

Article history:
Received 15 April 2008
Received in revised form 15 May 2008
Accepted 24 May 2008
Available online 8 June 2008

Keywords:
Solid oxide fuel cell
Interconnect
Oxidation
Coating
Resistivity

ABSTRACT

In solid oxide fuel cells (SOFC) for operating temperatures of 800 °C or below, the interconnection plates can be made from stainless steel. This is a big economic advantage, but energy losses can be caused by undesirable reactions between the alloys and other SOFC components. The use of coatings on interconnect stainless steels can reduce this degradation. A $MnCo_{1.9}Fe_{0.1}O_4$ (MCF) spinel not only significantly decreases the contact resistance between a $La_{0.8}Sr_{0.2}FeO_3$ cathode and a stainless steel interconnect, but also acts as a diffusion barrier to prevent Cr outward migration through the coating. The level of improvement in electrical performance depends on the ferritic substrate composition. For Crofer22APU and F18TNb, with a Mn concentration of 0.4 and 0.12 wt%, respectively, the reduction in contact resistance is significant. In comparison, limited improvement is achieved by application of MCF on IT-11 and E-Brite containing no Mn. No influence of the minor additions of Si or Al is observed on contact resistance. The MCF protection layer bonds well to the stainless steel substrates under thermal cycling, but the thermal expansion difference is too large between the $La_{0.8}Sr_{0.2}Co_{0.75}Fe_{0.25}O_3$ contact layer used and Crofer22APU and IT-11.

1. Introduction

The SOFC designed by Ikerlan for an operating temperature of 600–800 °C is a metal-supported tubular fuel cell [1,2], developed to be used for electricity and heat generation in domestic systems. This electrochemical device will operate at temperatures below 800 °C, allowing the ceramic components to be replaced, i.e. $LaCrO_3$, by metallic materials as current collectors [3–5]. Several earlier publications were dedicated to cathode current collectors [3,4,6]. The characteristics of these current collectors are the following:

1- Compatibility of the thermal expansion coefficient with that of the ceramic components, i.e. electrolyte material (yttria-stabilised zirconia YSZ, $10.5 \times 10^{-6}\ K^{-1}$ between 20 and 1000 °C [3,4]) and cathode material (strontium-substituted lanthanum ferrite, $La_{0.8}Sr_{0.2}FeO_3$, $13.3 \times 10^{-6}\ K^{-1}$ [7]).
2- High electronic conductivity in cathode atmosphere. In the case of oxides with low conductivity, the oxide scale should be modified or should have a slow growth rate [8,9].
3- Very low chemical reactivity with the cathode material and no chromium evaporation at the operating temperature.
4- The interconnect should be easy to manufacture, which is a key point in determining the feasibility of large-scale manufacturing.
5- The cost of raw materials as well as manufacturing processes for the interconnect also need to be as low as possible so that they will not present major obstacles to commercialization. A reduction in the cost of the interconnect especially is of particular significance for the metal-supported tubular SOFC.

Ferritic steels with more than 16% of chromium content are the most desirable materials combining most of these properties [3]. A disadvantage of the metallic interconnects is the formation of oxide scales leading to significant ohmic losses. The oxidation of steels can be improved, and many studies reported on the effect of small amounts of alloyed elements in oxidation, demonstrating that the oxidation of steels does not only depend on the Cr content. The most commonly used reactive elements (RE), which are added in concentrations of a few hundreds or tenths of a percent, are Y, La, Ce and Nd as metallic or oxide particles. Apart from improved oxide scale adhesion, the RE addition leads to a substantial decrease in oxide growth rate [10,11] and in the case of low Cr alloys they promote the selective oxidation of chromium [12]. If the RE is added

* Corresponding author at: Ikerlan-Energia, Parque Tecnologico de Alava, Juan de La Cierva 1, 01501 Miñano, Spain. Tel.: +34 945297032; fax: +34 945296926.
E-mail address: xmontero@ikerlan.es (X. Montero).

0378-7753/$ – see front matter © 2008 Elsevier B.V. All rights reserved.
doi:10.1016/j.jpowsour.2008.05.081

Table 1
Composition of the steels in weight%

	Fe	Cr	Mn	Ti	Si	Al	Mo	Others
Crofer22APU	76.45	22.78	0.4	0.07	0.02	0.006	–	La 0.086
F18TNb	78	19.4	0.12	0.12	0.46	0.02	1.7	Nb 0.17
IT-11	71.8	26.4	n.a.	n.a.	0.01	0.02	n.a.	Y 0.08
E-Brite	73.2	24.1	0.04	0.01	0.19	0.02	0.96	–

in the form of an oxide dispersion, it not only improves the oxidation resistance, but it also has a positive effect on the mechanical properties, especially creep resistance [12,13].

Crofer22APU, F18TNb, IT-11 and E-Brite are ferritic steels and have been selected from among a large number of possible materials showing the aforementioned characteristics. IT-11 and the E-Brite have been chosen due to their low and high impurities of Si and Al, respectively, and are known to form a Cr_2O_3 layer [14–16]. Crofer22APU and F18TNb have also been selected because of their low and high Si and Al contents, respectively. However, these two steels contain a small amount of Mn, which favours the formation of two oxides layers composed of chromium oxide and an outside layer of manganese chromium spinel [16].

Several disadvantages have been observed when ferritic steels were used as a cathode current collector. The Cr migration they show, by evaporation or diffusion, degrades the electrochemical properties of the SOFC by decomposition of the cathode or deposition at the active sites of oxygen reduction [17–19]. It has been demonstrated that the steels forming $MnCr_2O_4/Cr_2O_3$ oxide layers under oxidising SOFC operating conditions, substantially reduce the Cr evaporation [20]. However, a further improvement of Cr retention can be achieved by coating the interconnect with spinel-forming elements such as cobalt manganese spinels [21–23].

Interaction of the metallic interconnects with the adjacent ceramic cell components and the resulting stable time-dependent resistance of these material combinations is highly important. To address the latter problem, contact materials are used in stack assembly for better electrical contact between the interconnects and the electrodes and also for compensation of dimensional tolerances of the parts. Such contact layers have no direct role in electrochemical reaction, but they can provide a homogeneous contact over the whole area of the fuel cell and minimise the ohmic losses within the stack. A chemical interaction between the contact layer and an electrode or the interconnect should not occur, but cannot be avoided in most cases due to the reaction of the contact material with the chromia scale formed on the interconnect.

This work presents the effect of a $MnCo_{1.9}Fe_{0.1}O_4$ spinel as protective coating and $La_{0.8}Sr_{0.2}Co_{0.75}Fe_{0.25}O_3$ perovskite as a contact layer in combination with several commercial ferritic steels at 800 °C. Analyses of the structural evolution were carried out by electron microscopy when samples were oxidized isothermally and cyclically in order to observe reactions and mechanical stability between the alloys and the applied layers. In addition, contact resistance measurements between the coated alloys and the $La_{0.8}Sr_{0.2}FeO_3$ cathode were performed by 4 point DC up to 1000 h.

2. Experimental procedure

Four commercial steels were investigated at 800 °C: Crofer22APU (ThyssenKrupp VDM, Werdohl, Germany), F18TNb (Ugine Arcelor, Isbergues, France), IT-11 (Plansee AG, Reutte, Austria) and E-Brite (Allegheny-Lludlum, Pittsburg, USA). The composition of the steels, given by the suppliers, is listed in Table 1. Even if the envisaged SOFC is tubular-shaped, all the tests were carried out with flat samples for an easier experimental mounting and characterisation.

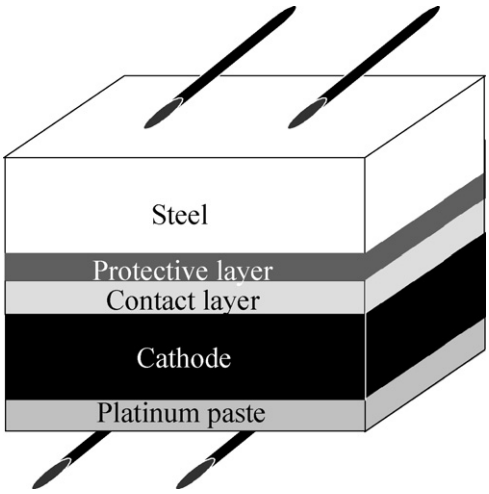

Fig. 1. Sample setup for ASR measurements for steel-cathode contact resistances.

Area specific resistance (ASR) measurements were carried out as shown in Fig. 1. The alloys were cut in $10 \times 10 \times 1\,mm^3$ pieces, polished and cleaned before coating. The protective layer against Cr poisoning was prepared by slurry coating of $MnCo_{1.9}Fe_{0.1}O_4$ (MCF) spinel powders [24], supplied by HC Starck (Goslar, Germany). The MCF ink was applied by screen-printing onto the different steels (approximately 60 μm of thickness before drying). The densification of the applied spinel coating was realised by reactive sintering at 800 °C. For this purpose, the coated steel was exposed to a reducing atmosphere of 10^{-18} bar oxygen partial pressure, obtained by an Ar/3% H_2O/4% H_2 gas mixture, for 2 h and after the reducing heat-treatment, reoxidized during 10 h in air for obtaining again a spinel structure [23,25]. The spinels were analysed before and after densification by X-ray diffraction (XRD; Siemens D500). After densification of this layer, a $La_{0.8}Sr_{0.2}Co_{0.75}Fe_{0.25}O_3$ (LSCF) [26] contact layer was applied to ensure a good contact with the $La_{0.8}Sr_{0.2}FeO_3$ (LSF) cathode substrate (Fig. 1), also by screen-printing (approximately 160 μm before drying). The perovskite powders were produced by the Pechini method [27]. The LSF powder was produced by spray pyrolysis and their pellets were manufactured by the Coat-Mix® method [28] and sintered at 1100 °C. The assembling of the coated steels with the LSF cathode was carried out by a heat-treatment in air at 850 °C for 10 h. A weight of $0.5\,kg\,cm^{-2}$ was uniformly loaded onto the samples in order to achieve a better mechanical contact during measurement. Current density of $0.3\,A\,cm^{-2}$ was applied during the resistance measurement by 4 point DC setup for up to 1000 h.

The microstructure and composition of the samples after ASR measurement was characterised by scanning electron microscopy (SEM) (Zeiss Ultra55) combined with energy dispersive X-ray spectroscopy (EDX) on cross-sections of the specimens.

Finally, the thermo-mechanical stability of the densified spinel protection layer on the steels with and without perovskite contact layer was evaluated by cyclic oxidation tests. For this purpose six samples, two of Crofer22APU, F18TNb and IT-11 each, were cut in $50 \times 20 \times 1\,mm^3$ pieces, polished with 1200 SiC grit, and screen-printed with MCF. After heat-treatment at 800 °C for densification, one piece of every steel was coated with LSCF contact layer and the other remained uncoated. Visual inspection of the samples took place after 43 cycles of 23 h at 800 °C and 1 h at room temperature, representing approximately 1000 h at 800 °C. Samples were instantaneously heated and cooled during the cycles by putting them into and taking them out of the furnace without special attention to cooling or heating rates.

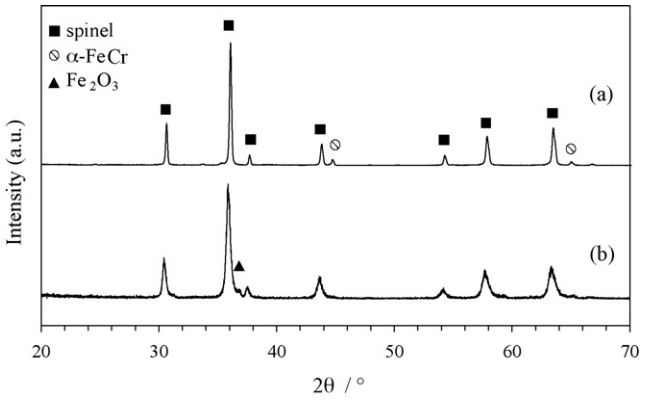

Fig. 2. XRD patterns of MCF powder after calcination at 750 °C (a) and after densification and 300 h of oxidation in air on Crofer22APU (b).

3. Results and discussion

3.1. Evolution of spinel coating on ferritic steels

Fig. 2 shows the XRD pattern of the MCF powder after powder preparation in comparison to the MCF-coated on Crofer22APU after reactive sintering and 300 h of oxidation in air. The lattice parameter remained unchanged in both cases, 8.309 and 8.307 Å, respectively. After powder preparation, Fe_2O_3 was detected as an impurity. In the pattern after 300 h of oxidation in air α-FeCr from the steel is detected. In comparison to $MnCo_2O_4$, a slight increase of the lattice parameter was observed (a = 8.28 Å, JCPDS no. 01-084-0482) in both cases shown in Fig. 2. This increase is likely due to the partial substitution of iron in the spinel as no Cr was detected in the spinel before reactive sintering. Cr substitution in this spinel might also lead to an increase in lattice parameter, because $(Mn,Cr)_3O_4$ spinels have lattice parameters in the range of 8.43–8.47 Å (JCPDS no. 01-075-1614 and 01-071-0982). However, it cannot be excluded that the small difference in lattice parameter is the result of a partial substitution of Cr in the spinel during the heat-treatments.

Fig. 3 shows the SEM cross-section analysis of MCF-coated Crofer22APU after reactive densification at 800 °C in air. The spinel layer was well-bonded to the substrate and free of Cr. Remaining porosity is still present in the spinel layer and a reaction zone of around 1 μm was generated between the spinel layer and the substrate, characterised by a sharp Cr gradient and composed of a chromium–cobalt–manganese spinel.

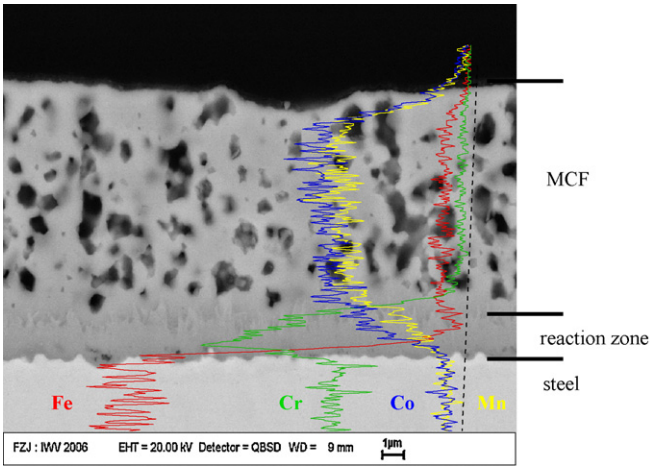

Fig. 3. SEM cross-section of Crofer22APU coated with MCF after reactive sintering at 800 °C. Inserted EDX line-scan with Cr, white line with symbols; Mn, white line; Co, black line with symbols; Fe, black line.

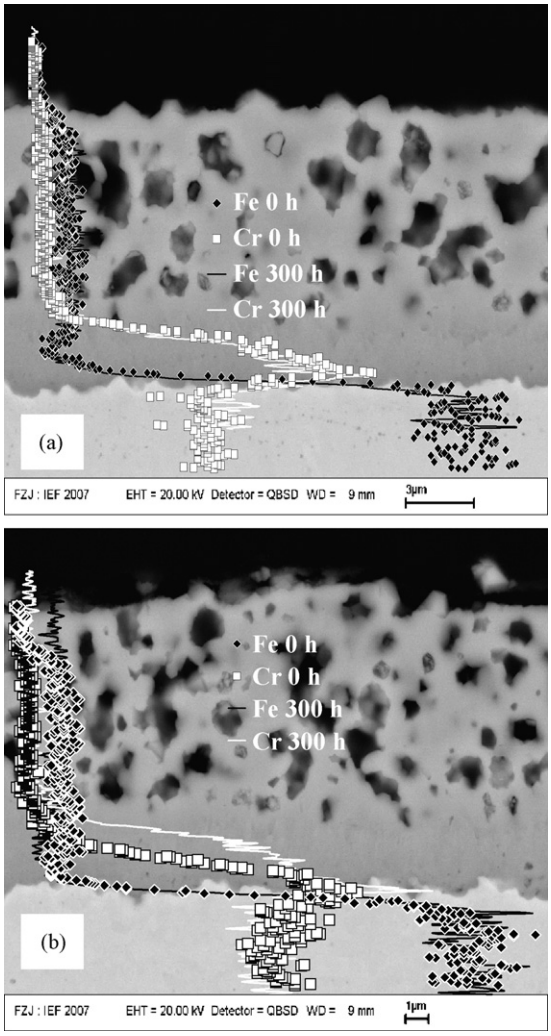

Fig. 4. SEM cross-section of densified spinel coating on Crofer22APU (a) and IT-11 (b) after 300 h in air at 800 °C. Inserted EDX line-scan shows the profiles of Fe and Cr just after densification and after 300 h in air at 800 °C.

After 300 h of oxidation in air (Fig. 4a), the coating is still well-bonded to the substrate and free from cracks. Outside of the reaction zone, the Cr content is still below the detection limit of EDX analysis. The pores seem to be agglomerated. No composition or thickness variation was observed at the reaction zone.

The cross-section analysis of the coated IT-11 after 300 h of oxidation in air (Fig. 4b), reveals the same microstructural changes in porosity as in the case of Crofer22APU. No Cr was observed in the coating and good adherence was achieved, but in contrast to the Crofer22APU sample, the reaction zone shows an increase in thickness and consequently a higher Cr amount. The chromia growth on IT-11 is three times slower than the growth on Crofer22APU in air at 800 °C [13,15]. Hence, the observed increase in thickness cannot be related to the chromia growth on the steel.

For a better explanation of the changes observed in the reaction zone of IT-11, the SEM cross-section of the substrate with densified spinel before and after 300 h of oxidation in air at 800 °C is compared in Fig. 5. The formation of σ-phase, rich in chromium and molybdenum, within the substrate (grains with bright colour) can be seen here, as well as the evolution of this phase with time. The σ-phase was not detected before thermal treatment and the

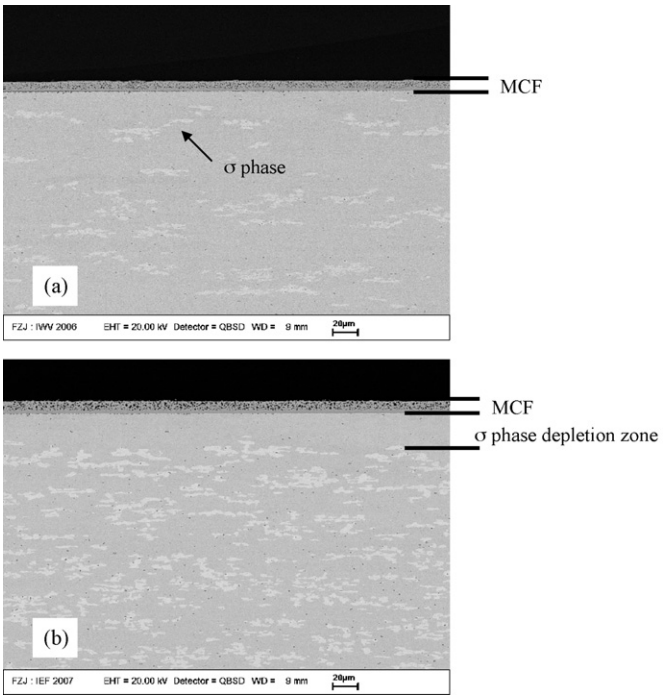

Fig. 5. SEM cross-section of IT-11 coated with MCF after reactive sintering (a) and after 300 h in air at 800 °C (b).

amount of transformed phase increases with oxidation time, creating elongated grains oriented parallel to the steel surface. The sample oxidized after 300 h at 800 °C (Fig. 5b), shows a depleted zone of σ-phase of more than 20 μm deep beneath the spinel coating. This could be related to the formation and simultaneous oxidation of the σ-phase [29]. The Cr originally retained in the σ-phase diffuses to the steel surface and enriches the reaction zone in chromium and depletes the σ-phase within the steel.

3.2. ASR of Crofer22APU-LSCF-LSF with and without MCF protection layer

As shown in Fig. 6, after temperature stabilisation, the ASR of the uncoated sample increased from 70 to 80 mΩ cm^2 during 260 h with a relatively high rate when the contact layer is in direct contact with the steel. The application of the MCF protective layer led to a

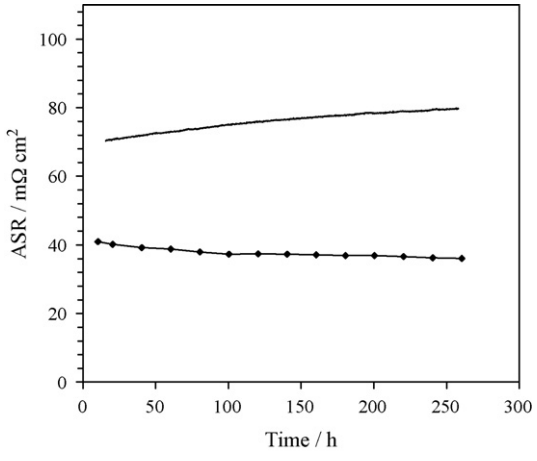

Fig. 6. ASR of Crofer22APU-LSCF-LSF (line without symbols) and Crofer22APU-MCF-LSCF-LSF (line with symbols) as function of time.

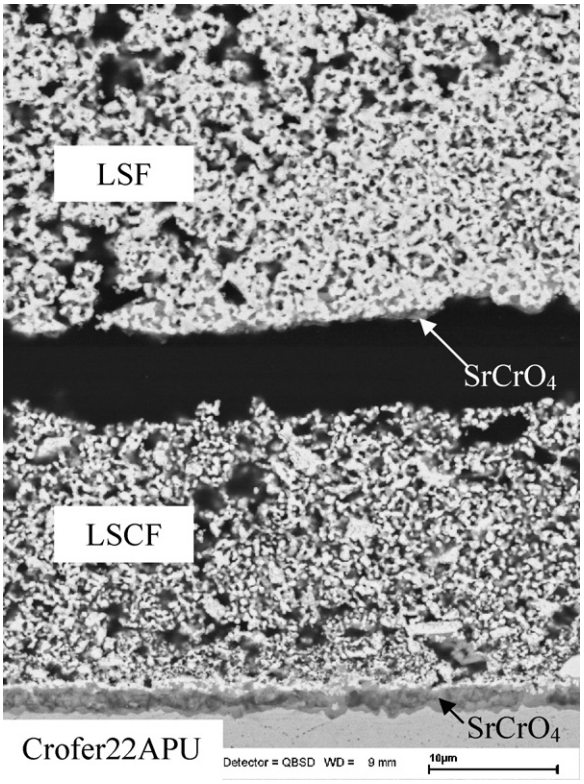

Fig. 7. SEM cross-section of Crofer22APU-LSCF-LSF without protective layer after 260 h in air at 800 °C.

reduction in the contact resistance between LSF and Crofer22APU showing around 41 mΩ cm^2 after temperature stabilisation, followed by a slow decrease during the first 260 h to 36 mΩ cm^2. The reduction in ASR is mainly attributed to an improved chemical compatibility of the contact material with the spinel protection layer compared to its compatibility with Crofer22APU, i.e. the scale grown on the metal [23].

The interaction between Crofer22APU and LSCF contact material is shown in Fig. 7. The contact layer was well adhered to the metallic substrate but the cathode was not attached after the measurement. A continuous $SrCrO_4$ layer was formed at the interfaces between Crofer22APU/LSCF and LSCF/LSF and $SrCrO_4$ was also found within the contact layer and the LSF cathode. A thin and uniform lanthanum strontium chromite layer (white coloured layer in Fig. 7) was formed between the applied LSCF contact layer and the $SrCrO_4$ continuous layer on the steel. The increase observed in the ASR measurement of the uncoated sample is attributed to the formation of these two layers with lower conductivity compared to MCF. It is interesting to note that the use of $La_{0.8}Sr_{0.2}Co_{0.5}Mn_{0.5}O_3$ as a contact layer [30] did not show this pronounced formation of $SrCrO_4$. This is an additional indication that LSCF perovskites exhibit the tendency of easier release of strontium from the crystalline lattice than manganite-based perovskites [31].

3.3. ASR of ferritic steels with MCF protection layer and LSCF contact layer

The evolution of contact resistance over time of the four selected alloys in combination with MCF, LSCF and LSF up to 1000 h is shown in Fig. 8.

Assuming a linear evolution of the measured resistivity over the time, the ASR curves can be divided into two time-dependent intervals, an initial period in which the interaction between the applied

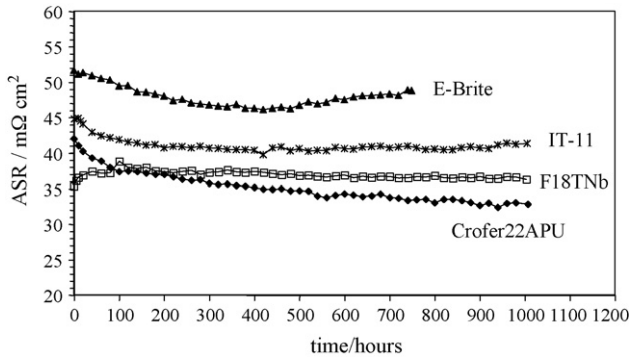

Fig. 8. ASR of Crofer22APU, F18TNb, IT-11, E-Brite coated with MCF spinel and LSCF contact layer.

layers with the steels occur (interval A) and a long-term exposure period (interval B), in which an interaction between the applied spinel and the contact layer occurs and the main process is the oxide scale growth beneath the MCF coating. The duration of the periods and their time-dependent behaviour depends on the steel composition. For E-Brite, the initial period was estimated around 360 h and for Crofer22APU, IT-11 and F18TNb around 120 h. The ASR was decreasing in this period for all the steels except for the F18TNb. In the second period, the ASR values decreased for F18TNb and Crofer22APU, remains stable for IT-11 and increases for E-Brite. The initial resistivity value and the ASR slopes for the described periods are listed in Table 2.

After the ASR measurements, SEM analysis on the cross-sections of the tested samples (Fig. 9) indicated that the spinel coatings were well-bonded to the ferritic substrates and free from spallation but with remaining porosity. White-coloured La-rich and grey-coloured Co-rich agglomerations were observed in the LSCF contact layers, probably due to an incomplete reaction or excess of La during powder preparation.

For the coated Crofer22APU, a chromia scale about 0.4 μm thick (measured directly from the SEM image) was grown between the metal substrate and the MCF coating. With EDX no evidence of Cr penetration thought the spinel coating was found either into the LSCF contact layer or into the LSF cathode. Loss of adherence was

Table 2
Resistivity and resistivity slopes describing the time-dependent ASR measurements

	Crofer22APU without MCF	E-Brite	IT-11	Crofer22APU	F18TNb
Initial resistivity ($m\Omega\,cm^2$)	70.9	51.7	44.8	41.7	35.3
Slope during interval A ($m\Omega\,cm^2\,h^{-1}$) $\times 10^3$	51.1	−14.9	−30.0	−38.6	19.7
Resistivity at the beginning of interval B ($m\Omega\,cm^2$)	78.2	46.9	41.5	37.4	37.9
Slope during interval B ($m\Omega\,cm^2\,h^{-1}$) $\times 10^3$	26.5	6.9	−0.2	−5.2	−1.5

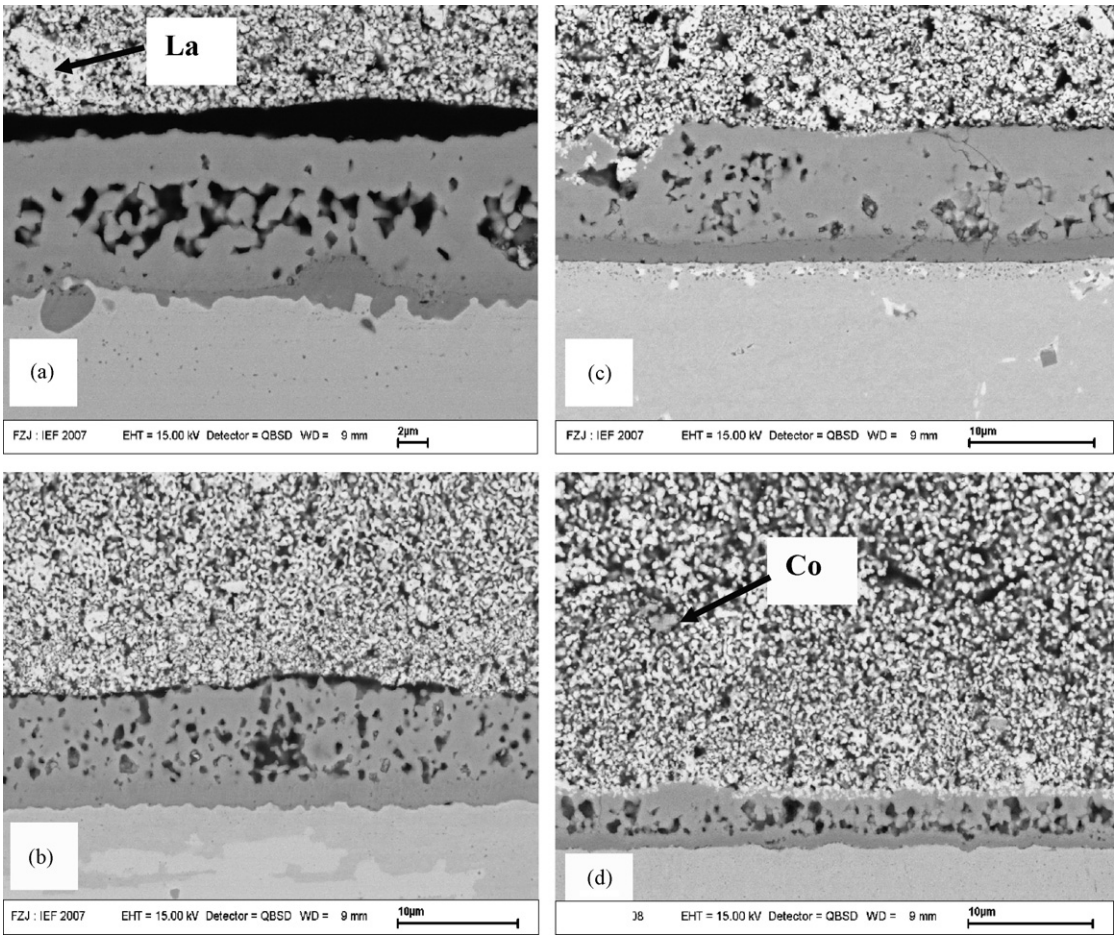

Fig. 9. SEM cross-section of Crofer22APU (a), IT-11 (b), F18TNb (c) and E-Brite (d), coated with MCF protective layer and LSCF contact layer after 4 point DC resistivity measurement in combination with LSF cathode.

Table 3
Chromia layer thickness in μm after 1000 h of oxidation in air at 800 °C

	MCF	Without MCF [34]
Crofer22APU	0.4	0.4
F18TNb	2	1.8
IT-11	0.28	0.2
E-Brite	0.75	0.68

observed between the protection and contact layer during cooling down to room temperature.

The SEM cross-section of the coated F18TNb showed that a chromia scale with about 2 μm thickness was grown between the ferritic substrate and the MCF coating. The protection layer was again well adherent to the substrate. Some cracks were observed in the coating at regions with high densification. Therefore, the closed pore microstructure observed in the case of Crofer22APU may also be beneficial by providing strain tolerance to improve thermo-mechanical stability during SOFC operation. A reaction zone was detected under the applied spinel layer and both EDX point and line analyses found no evidence of Cr penetration through the coating into the LSCF contact or the LSF cathode. The EDX analysis, however, showed segregation of Si, likely in the form of silica, at the interface between the corrosion scale and the metal substrate but no evidence of spallation was detected at least during the duration of this test. There was also no loss of adherence between the LSF cathode and contact layer after cooling down to room temperature.

For the coated IT-11, the SEM analysis of the cross-section indicated that the spinel coating was well-bonded to the substrate and free from spallation or cracks. A thin chromia scale was observed between the MCF coating and substrate alloy (0.28 μm), and a Cr enriched reaction zone (1.85 μm) was detected as a reaction zone with the MCF. Apart from this, no evidence of Cr penetration through the spinel coating into LSCF contact layer or LSF cathode was detected, and the contact layer did not spall off from the cathode after cooling down.

Finally for the coated E-Brite, the cross-section analysis indicated that the spinel coating was also well-bonded to the substrate. A thin chromia scale was observed between the coating and the substrate (0.75 μm). Beneath the formed oxide scale, a silica layer was formed, which similarly to F18TNb did not affect the adherence of the MCF coating, at least during the 1000 h of exposure time. No evidence of Cr penetration through the spinel coating into the LSCF contact layer or the LSF cathode was detected, and the contact layer adhered to the cathode after cooling down.

The MCF spinel protection layer did not apparently affect the growth rate of the chromia scale formed on the different metal substrates, which evolved very similarly to those observed for the same conditions and time during isothermal tests at 800 °C as listed in Table 3.

The initial high resistivity observed for E-Brite and IT-11 (see Table 2) is related to the high Cr and lack of Mn content of these steels. During the sintering process of the applied spinel coating in reducing atmosphere, the released Cr and the reduced Co can form a Cr–Co spinel reaction zone between the steel and the MCF coating, whereas the reaction zone of Crofer22APU and F18TNb is formed with lower Cr content and results in a Cr–Co–Mn spinel. Pirón-Abellán and cowokers [20] showed that very short oxidation times are necessary to form a Mn–Cr spinel at the Crofer22APU surface. This spinel, which is also stable in the reductive sintering conditions, decreases the Cr release from the steel, forming a lower Cr-containing Mn–Co–Cr spinel on F18TNb and Crofer22APU. Different groups have also reported that a high content of Cr and/or a low content of Mn in Mn–Co–Cr spinels decrease the conductivity [33,34]. Therefore, the initial values of the observed resistivities are dominated by the composition of the reaction zone formed during the densification of the applied MCF spinel, which is directly related to the Cr and Mn content of the steels. The Cr content and the initial ASR is the lowest for the F18TNb followed by Crofer22APU which contains 3% more Cr than F18TNb. The third was IT-11, which contains a higher amount of Cr than E-Brite, but differently to this, IT-11 also contains a very low amount of Mn (even if it is not specified by the supplier), showing consequently for the E-Brite the highest initial resistivity value.

The composition of the spinel formed at the reaction zone is modified during the ASR measurement and dominates the resistivity evolution during the first interval A. These compositional changes are related to the Mn and Cr diffusing from substrate steels, leading to a spinel with similar composition for Crofer22APU and F18TNb, and hence a similar resistivity (see the values in the beginning of interval B summarised in Table 2). The conductivity of the spinels formed in the reaction zone after interval A for IT-11 and E-Brite remains lower due to the aforementioned low Mn content of these steels.

In the analysis of the interface between the protective and contact layer after 1000 h of exposure time (Fig. 9), a fine-grained region was observed in the contact layer above the MCF spinel for all the studied samples. This fine-grained zone always revealed Mn by EDX, which was initially not present in the contact layer. As reported by Tietz et al. [26], $La_{0.8}Sr_{0.2}(Co,Fe)O_3$ perovskites possess a higher conductivity than similar $La_{0.8}Sr_{0.2}(Co,Fe,Mn)O_3$ perovskites. But also several beneficial effects are related to the incorporation of the Mn into this contact layer perovskite: the reduction of the thermal expansion coefficient, which may improve the adherence between the contact layer and the protection layer, and an improvement in the electrical contact due to the finer grain size of the newly formed perovskite.

The combination of the oxide scale growth rates and the Mn and Cr content in the reaction zone the composition of which changes during the test, and the aforementioned interaction between the MCF spinel and the LSCF, determine the different evolutions of ASR observed during long-term exposures (interval B). For the Crofer22APU the highest decrease in resistivity was observed due to the low growth rate of the oxide scale shown usually by this alloy [32] and the high amount of Mn in the steel, which leads to a low Cr and high Mn containing spinel reaction zone. The F18TNb, showing similar characteristics to Crofer22APU, has a higher oxide growth rate, which is apparently the reason for showing a lower rate of resistivity decrease. Even if the oxide growth rate for IT-11 is the lowest among the four steels compared [32], it showed an initial high Cr-containing reaction zone and increasing resistance values with time. The benefit of having the lowest oxide scale growth rate does not seem to be the determining property for achieving low ASR values. Finally the E-Brite showed the highest ASR and the strongest increase of ASR because of the high Cr content in the reaction zone and the high oxide scale growth rate [32].

3.4. Thermo-mechanical stability of the applied coatings after cyclic oxidation test

The thermo-mechanical stability of the densified spinel protection layer on ferritic steels with and without a perovskite contact layer was evaluated by cyclic oxidation tests. For this purpose only Crofer22APU, F18TNb and IT-11 were tested, as these steels showed the lowest degradation after ASR measurement and microstructure analysis.

When no contact layer was applied, an excellent stability for all the substrates and no spallation or chipping was observed (Fig. 10). In contrast, chipping was observed after 1000 h of cyclic oxidation on Crofer22APU and IT-11 when the contact layer was applied.

Fig. 10. Samples of Crofer22APU (left), IT-11 (right) and F18TNb (middle) coated with densified MCF (top) and coated with densified MCF and LSCF contact layer (bottom) after 1000 h of cyclic test at 800 °C in air.

Table 4
Thermal expansion coefficients (TEC) of the materials used in the cyclic test

	Crofer22APU	F18TNb	IT-11	MCF	LSCF
TEC 10^{-6} K^{-1} (30–800 °C)	11.9 [35]	12.8 [36]	11.6 [17]	13.4 [26]	19 [28]

The average thermal expansion coefficients of the materials used for the cyclic test are listed in Table 4. Apparently the thermal expansion match between the MCF spinel layer and the LSCF perovskite is insufficient. Presumably it is also insufficient between the contact layer and the LSF cathode (13.3×10^{-6} K^{-1} [7]). Therefore, the use of the LSCF contact layer seems to be detrimental if the application of the SOFC is oriented to a high thermal cyclability and when the stack is not permanently exposed to compressive stresses.

4. Conclusions

A protection layer of $MnCo_{1.9}Fe_{0.1}O_4$ spinel can be densified on ferritic steels by reactive sintering at 800 °C. The densified spinel layer does not only significantly decrease the contact resistance between an LSF cathode and the steel interconnect, it can also act effectively as a barrier to outward diffusion of chromium cations, preventing subsequent chromium migration into the cathode and contact material.

The evolution of ASR depended on the ferritic substrate composition. For Crofer22APU and F18TNb with a relatively high Mn concentration, a decrease in contact resistance was observed. Limited improvement was achieved by the application of the spinel coating on IT-11 and E-Brite, which contain low or no Mn, respectively. The residual Si and Al amounts in F18TNb and E-Brite did not cause any spallation of oxide scale or protection layer and no apparent conductivity decrease during the 1000 h of exposure.

The combination of good matching of thermal expansion between the spinel and the ferritic steel as well as the densified microstructure may contribute to the observed excellent structural and thermo-mechanical stability of these spinel protection layers. However, the thermal expansion match between the spinel and $La_{0.8}Sr_{0.2}Co_{0.75}Fe_{0.25}O_3$ contact layer seems to be insufficient for thermal cycling.

Acknowledgements

The materials in this work were provided by the Real-SOFC program which the author gratefully acknowledges. This work was financially supported by the strategic action GENEDIS (Etortek) of the Basque Country Government. The author wants to thank W. Fischer (FZJ, IEF-2) for the XRD analyses. X. Montero also thanks IEF-1 as host institution for continuous support of his PhD work.

References

[1] I. Villarreal, C. Jacobson, A. Leming, Y. Matus, S. Visco, L. De Jonghe, Electrochem. Solid State Lett. 6 (2003) A178.
[2] I. Antepara, I. Villarreal, L.M. Rodríguez-Martínez, N. Lecanda, U. Castro, A. Laresgoiti, J. Power Sources 151 (2005) 103.
[3] K. Hilpert, W.J. Quaddakers, L. Singheiser, Interconnects, vol. 4. Part 8. Handbook of Fuel Cells-Fundamentals, Technology and Applications, John Wiley & Sons, Ltd, Chichester, 2003, pp. 1037–1054.
[4] J.W. Fergus, Mater. Sci. Eng. A 397 (2005) 271.
[5] Z. Yang, K. Scott Weil, D.M. Paxton, J.W. Stevenson, J. Electrochem. Soc. 150 (2003) A1188.
[6] H.U. Anderson, F. Tietz, Interconnects, in: S.C. Singhal, K. Kendall (Eds.), High Temperature Solid Oxide Fuel Cells, Fundamentals, Design and Applications, Elsevier Science, The Netherlands, 2004, Chapter 7.
[7] A. Mai, Ph.D. thesis, Katalytische und electrochemische Eigenschaften von eisen- und kobalt- haltigen Perowskiten als Kathoden für die oxidkeramische Brennstoffzelle (SOFC), Ruhr Universitat, Bochum (2004).
[8] W.J. Quadakkers, T. Malkow, J. Pirón-Abellán, U. Flesch, V. Shemet, L. Singheiser, in: A.J. McEvoy (Ed.), Proceedings of the 4th European Solid Oxide Fuel Cell Forum, Lucerne, Switzerland, 2000, p. 827.
[9] S. Genj, J. Zhu, J. Power Sources 160 (2006) 1009.
[10] H.S. Seo, G. Jin, J.H. Jun, D. Kim, K.Y. Kim, J. Power Sources 178 (2008) 1.
[11] P. Hou, J. Stringer, J. Electrochem. Soc. 134 (1987) 1836.
[12] W.J. Quadakkers, J. Pirón-Abellán, V. Shemet, L. Singheiser, Mater. High Temp. 20 (2003) 115.
[13] W. Glatz, G. Kunschert, M. Janousek, A. Venskutonis, in: S.C. Singhal, J. Mizusaki (Eds.), Proceedings of the Ninth International Symposia on Solid Oxide Fuel Cells (SOFC-IX), vol. 2005-07, The Electrochemical Society, Pennington, NJ, USA, 2005, p. 1773.
[14] M. Stanislowski, E. Wessel, K. Hilpert, T. Markus, L. Singheiser, J. Electrochem. Soc. 154 (2007) A295.
[15] W. Glatz, G. Kunschert, M. Janousek, in: M. Mogensen (Ed.), Proceedings of the 6th European Solid Oxide Fuel Cell forum, Lucerne, Switzerland, 2004, p. 1612.
[16] Z. Yang, J.S. Hardy, M.S. Walker, G. Xia, S.P. Simner, J.W. Stevenson, J. Electrochem. Soc. 151 (2004) A1825.
[17] K. Fujita, T. Hashimoto, K. Ogasawara, H. Kameda, Y. Matsuzaki, T. Sakurai, J. Power Sources 131 (2004) 270.
[18] E. Konysheva, H. Penkalla, E. Wessel, J. Mertens, U. Seeling, L. Singheiser, K. Hilpert, J. Electrochem. Soc. 153 (2006) A765.
[19] S.P. Jiang, J.P. Zhang, X.G. Zheng, J. Eur. Ceram. Soc 22 (2002) 361.
[20] P. Huczkowski, N. Christiansen, V. Shemet, L. Niewolak, J. Pirón-Abellan, L. Singheiser, W.J. Quadakkers, Fuel Cells 6 (2006) 93.
[21] Y. Larring, T. Norby, J. Electrochem. Soc. 147 (2000) 3251.

[22] T. Kiefer, M. Zahid, F. Tietz, H.R. S Zerfass, Proceedings of the 7th European Solid Oxide Fuel Cell Forum European Fuel Cell Forum, Oberrohdorf, Switzerland, 2006, File No. B0803.
[23] Z. Yang, G. Xia, S.P. Simner, J.W. Stevenson, J. Electrochem. Soc. 152 (2005) A1896.
[24] T. Kiefer, M. Zahid, F. Tietz, D. Stöver, H.R. Zerfass, in: S. Linderoth, A. Smith, N. Bonanos, A. Hagen, L. Mikkelsen, K. Kammer, D. Lybye, P.V. Hendriksen, F.W. Poulsen, M. Mogensen, W.G. Wang (Eds.), Proceedings of the 26th Risø International Symposium on: Solid State Electrochemistry, Roskilde, Denmark, 2005, p. 261.
[25] M.N. Rahaman, Ceramic Processing and Sintering, Marcel Dekker, Inc., New York, 1995.
[26] F. Tietz, I. Arul Raj, M. Zahid, D. Stöver, Solid State Ionics 177 (2006) 1753.
[27] M.P. Pechini, Patent No. 3,330,697, United States Patent Office.(1967).
[28] D. Simwonis, H. Thülen, F.J. Dias, A. Naoumidis, D. Stöver, J. Mater. Process. Technol. 92–93 (1999) 107.
[29] A.J. Strutt, K.S. Vecchio, Metall. Mater. Trans. A 30 (1999) 355.
[30] E. Konysheva, J. Laatsch, E. Wessel, F. Tietz, N. Christiansen, L. Singheiser, K. Hilpert, Solid State Ionics 177 (2006) 923.
[31] F. Tietz, et al., Solid State Ionics (2008) doi:10.1016/j.ssi.2007.11.037.
[32] X. Montero, F. Tietz, D. Stöver, M. Cassir, I. Villarreal, submitted to Corrosion Science.
[33] H. Ling, A. Petric, in: S.C. Singhal, J. Mizusaki (Eds.), Proceedings of the Ninth International Symposia on Solid Oxide Fuel Cells (SOFC-IX), vol. 2005-07, The Electrochemical Society, Pennington, NJ, USA, 2005, p. 1866.
[34] X. Chen, P.Y. Hou, C.P. Jacobson, S.J. Visco, L.C. De Jonghe, Solid State Ionics 176 (2005) 425.
[35] Crofer22APU, Material Data Sheet No. 8005, June 2004 edition, ThyssenKrupp VDM, Werdohl, Germany.
[36] F18TNb, Material Data Sheet, UGINOX. http://www.ugine-alz.com/uk/pdf/Fiches_techniques/F18TNb_uk.pdf.